CO Dissociation at Elevated Pressures on Supported Pd Nanoclusters

E. Ozensoy, B. K. Min, A. K. Santra, and D. W. Goodman*

Department of Chemistry, Texas A&M University, P.O. Box 30012, College Station, Texas 77842-3012

Received: July 29, 2003; In Final Form: December 9, 2003

In-situ polarization modulation infrared reflection absorption spectroscopy (PM-IRAS) is used to study CO adsorption at elevated pressures and temperatures on Pd nanoclusters deposited on crystalline SiO_2 thin films. The PM-IRAS data indicate that CO dissociates on the Pd nanoclusters at 185 mbar and at temperature >600 K. Combined STM and PM-IRAS data show that the Pd nanoclusters are three-dimensional and consist predominantly of ⟨111⟩ facets with an average diameter and height of 3.5 and 0.7 nm, respectively. STM data indicate no change in the morphology or sintering of the Pd nanoclusters between 300 and 650 K. For comparison, CO adsorption was investigated on a Pd(111) single-crystal surface using PM-IRAS under similar conditions (P_{CO} = 133 mbar, T = 175−750 K). Comparison of the PM-IRAS data for CO adsorption on Pd(111) and Pd nanoclusters indicate that in contrast to the Pd nanoclusters, CO adsorbs molecularly on the Pd(111) surface in a reversible manner, i.e., no dissociation.

I. Introduction

Recent advances in heterogeneous catalyst design have led to significant improvements in the reactivity and selectivity of automobile exhaust catalysts.[1,2] Further improvements will be greatly facilitated by developing a detailed understanding of the working catalyst surface at realistic reaction conditions.[3] Toward this goal, surface spectroscopies for use in real time at realistic conditions on complex model catalysts have been developed. Specific examples include recent studies at the gas−solid interface with scanning tunneling microscopy (STM),[4−6] sum frequency generation (SFG),[7] inelastic neutron scattering vibrational spectroscopy (INS),[8] and polarization modulation infrared reflection absorption spectroscopy (PM-IRAS).[9−15] In-situ studies of these kinds can greatly enhance our understanding of heterogeneous catalytic reactions at the molecular level.

Metal clusters on oxide supports are important in microelectronics fabrication, gas sensing, photovoltaic devices,[16] and heterogeneous catalysis. For example, three-way catalysts (TWC) consisting of Pd or Pt/Rh deposited on a high surface area metal-oxide support (typically γ-Al_2O_3) containing varying amounts of stabilizers and/or promoters such as CeO_2, SiO_2, La_2O_3, BaO are used in the selective reaction of CO, NO, and hydrocarbons in automobile catalytic converters.[17] In the mid-1990s, Pd-only catalysts began to displace Pt/Rh bimetallic TWC catalysts.[17] In these catalytic systems, as in any heterogeneous catalytic system, the metal cluster−support interaction, sintering, morphology, size, and cluster restructuring under catalytic conditions control the overall catalyst performance.

Recent advances in the synthesis of crystalline, ultrathin SiO_2 films have facilitated the study of metal nanoclusters on oxide supports using vibrational and electronic spectroscopies as well as scanning tunneling microscopy without the adverse affects of charging.[18−24] In the present study, STM and in-situ PM-IRAS have been combined to study CO adsorption on a complex model catalyst at elevated pressures (P_{CO} = 185 mbar) and temperatures (300−680 K). The model catalyst consists of Pd clusters deposited on a crystalline SiO_2 ultrathin film support grown on a Mo(112) substrate. These results are compared with our previous in-situ PM-IRAS results for CO adsorption on a Pd(111) single crystal at elevated pressures (10^{-6}−600 mbar) and temperatures (220 and 750 K).[9] PM-IRAS is an extremely versatile vibrational spectroscopic technique that can be used to investigate heterogeneous catalytic reactions at gas−solid interfaces at elevated pressures in real-time. Compared with sum frequency generation (SFG),[7] a nonlinear vibrational spectroscopic tool well-suited for use at realistic reaction conditions, PM-IRAS is considerably less expensive and less demanding experimentally, yet can provide comparable spectroscopic data that are straightforward to interpret.[9] The present study demonstrates for the first time that the PM-IRAS technique can be applied to three-dimensional nano-structures (in this case, Pd nanoclusters) allowing the effects of cluster size, morphology, and support interactions to be studied under realistic reaction conditions.

II. Experimental Section

PM-IRAS is surface sensitive because of the surface selection rules intrinsic to the reflection of infrared radiation from a conducting surface. Adsorbed species with a vibrational mode perpendicular to the surface plane are excited with light that is p-polarized but not with s-polarized light. Molecules in the gas or liquid phases that are isotropic absorb equally the s and p components of the incoming IR radiation. Using this disparity between the selection rules for surface adsorbates and the gas/liquid phase, a surface-specific vibrational spectrum of the adsorbed species, essentially independent of the ambient background, is acquired by measuring a differential reflectance spectrum ($\Delta R/R$) of the form $(p - s)/(p + s)$.[9−15]

The PM-IRAS data were taken in a combined ultrahigh vacuum (UHV)-microreactor system equipped with Auger electron spectroscopy (AES), temperature-programmed desorption (TPD) and low-energy electron diffraction (LEED). The UHV chamber has a base pressure of $\sim 6 \times 10^{-10}$ mbar; the pressure of the PM-IRAS microreactor (total volume ~ 300 mL) can be varied between 10^{-9} and 1000 mbar and is coupled to a FT-IR spectrometer (Bruker, Equinox 55). During acquisi-

* Author to whom correspondence should be addressed. E-mail: goodman@mail.chem.tamu.edu.

10.1021/jp030928o CCC: $27.50
Published on Web 03/17/2004

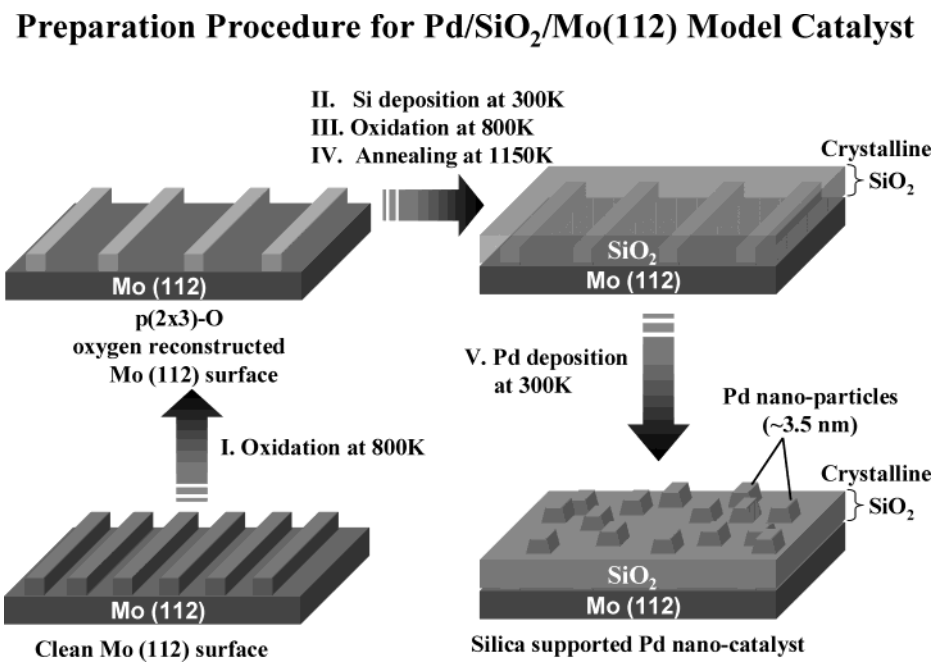

Figure 1. A schematic representation that summarizes the preparation procedure for a model catalyst consisting of Pd nanoclusters supported by a crystalline SiO_2 ultrathin film.

tion of the PM-IRAS data, the photoelastic modulator (PEM 90D, II/ZS50, 50 kHz, Hinds Instruments) was set to 1800 cm^{-1}, giving a spectral window between 1500 and 2300 cm^{-1}. PM-IRAS data were acquired at 4.5 min/spectrum (512 scans in the double-sided, forward−backward mode at 8 cm^{-1} resolution) at an angle of 85° from the surface normal using a liquid-nitrogen cooled MCT detector (D313/6-M, Infrared Associates, Inc.). Demodulation of the sum and difference spectral channels was carried out using a synchronous sampling demodulator (SSD-100-15, GWC Instruments). The Pd(111) crystal was cleaned by repeated cycles of oxidation at 650 K and subsequent annealing to 1200 K until its surface was found to be free of carbon, oxygen, and sulfur with AES. Carbon monoxide gas used in the adsorption experiments was research purity CO (>99.999%, Matheson-Trigas) and was further purified by cooling in liquid nitrogen prior to and during dosing. The purity of the gas was also confirmed prior to use with a quadruple mass spectrometer (QMS).

The STM experiments were carried out in a separate UHV chamber (base pressure ~5×10^{-10} mbar) equipped with STM, X-ray photoelectron spectroscopy (XPS), LEED, and AES. Typically the STM images were acquired in UHV in the constant current mode with a 1.5−2.5 V tip bias and ~0.1 nA tunneling current. Ultrahigh purity (99.999%) oxygen from MG industries and a Mo(112) crystal, oriented to <0.25° (from Matek, Germany), were used for the STM and PM-IRAS experiments. The Mo(112) surface was cleaned by oxygen treatment and high-temperature annealing (2100 K) until the carbon and oxygen AES signals were below the detectable level. Pd deposition on the SiO_2 ultrathin film was carried out using a Pd evaporation source consisting of a 0.25 mm Pd wire (99.997% Johnson Matthey Chemical Ltd.) wrapped around a tungsten filament. The Pd content of the model catalyst was checked with AES; an identical Pd coverage was used in the STM and PM-IRAS experiments.

III. Results

Several previous studies addressing the behavior of metal clusters on amorphous SiO_2 thin films supported on Mo(110) have been carried out in our laboratories using a variety of surface science probes.[25−27] Very recently, Freund and co-workers have reported the synthesis of ordered, epitaxial SiO_2 thin films on a Mo(112) surface.[18,19,21] By slightly modifying their preparation method,[19] SiO_2 thin films have also been prepared on a Mo(112) surface in our laboratories via vapor deposition of Si onto a p(2 × 3)-O oxygen-reconstructed Mo-(112) surface[20] followed by oxidation at 800 K and further annealing at 1150 K (Figure 1). In the initial stages of the SiO_2 thin film growth, superimposed LEED patterns with c(2 × 2) and p(n × 3) structures are observed and attributed to SiO_2 formation and reconstruction of the Mo(112) substrate, respectively. In addition, the terrace as well as the atomic row structure of this surface are very similar to the p(2 × 3) oxygen-induced reconstructed structure of the Mo(112) surface that is normally produced by oxidation between 800 and 900 K.[28] Accordingly, a p(2 × 3) O surface is considered to be a good template for SiO_2 thin film growth, and its presence is a key ingredient in the synthetic route to very reproducible and homogeneous SiO_2 thin films. A typical STM image (Figure 2a) of a SiO_2 thin film prepared by this recipe shows a very flat, homogeneous film with terrace structures coincident with the underlying Mo-(112) terraces. The Thickness of this SiO_2 film is estimated to be ~0.4 nm based on the AES intensity attenuation of the Mo substrate. In addition, the atomically resolved STM image of Figure 2b shows a c(2 × 2) structure that correlates identically with the sharp c(2 × 2) LEED structure observed for this surface. The unit cell spacing obtained from the STM image in Figure 2b is ~0.5 nm and consistent with the spacing derived from previous LEED studies for crystalline SiO_2 grown on Mo-(112).[18] Furthermore, ultraviolet photoelectron spectroscopy (UPS) and metastable impact electron spectroscopy (MIES) studies carried out in our laboratories on the SiO_2 thin films show a bulklike band gap (~8.8 eV).[22]

Figures 3a and 3b show the morphology of the Pd nanoclusters deposited on the SiO_2 thin film with a Pd coverage of 1.5 and 4 monolayer equivalents (MLE), respectively. The STM image of Figure 3a clearly shows that at a low Pd coverage (1.5 MLE), Pd nanoclusters exist randomly on the terraces and

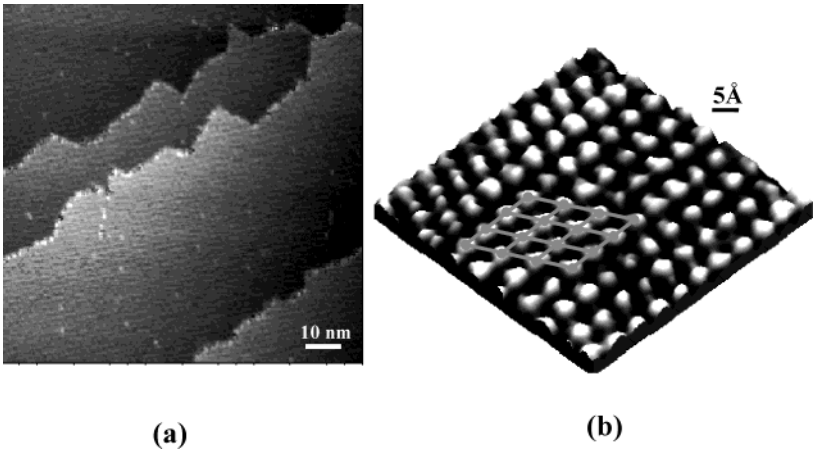

Figure 2. STM images obtained at 300 K in UHV for the crystalline SiO_2 ultrathin film grown on Mo(112). (a) STM image of a SiO_2 film corresponding to an area of 100 × 100 nm^2 (U_{tip} = +2.36 V, I_{tunnel} = 0.08 nA), (b) high-resolution STM image of a 5 × 5 nm^2 area of the SiO_2 film. (U_{tip} = +2.0 V, I_{tunnel} = 0.10 nA).

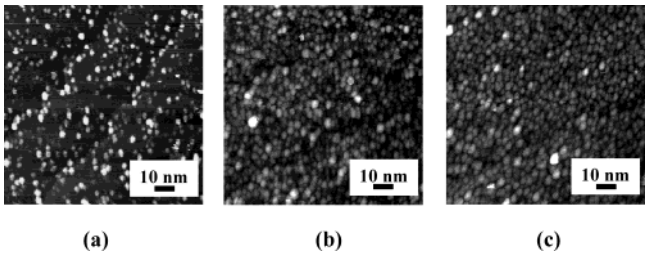

Figure 3. STM images showing various Pd loadings on SiO_2 and the behavior of the Pd nanoclusters with temperature. All of the STM images were acquired at 300 K for an area of 100 × 100 nm^2 in vacuum with U_{tip} = +1.70 V and I_{tunnel} = 0.08 nA. (a) Low Pd loading (~1.5 MLE) on SiO_2, (b) High Pd loading (~4 MLE) on SiO_2, (c) STM image obtained after surface (b) is annealed to 650 K and cooled back to 300 K.

the steps of the oxide support with a cluster size distribution between 1.5 and 3.5 nm. An increase in the Pd coverage to 4 MLE (see the STM image in Figure 3b) leads to an increase in cluster size (2.0−5.0 nm) and cluster density. However, the modest increase in the cluster size, in contrast to the large increase in cluster density with increasing Pd loading, implies that the Pd nanoclusters are relatively well-anchored to the SiO_2 substrate and are resistant to sintering at 300 K. The PM-IRAS experiments were carried out on those clusters depicted in Figure 3b.

Figure 3c shows the morphology of Pd nanoclusters after annealing at 650 K in vacuum. It is apparent from Figure 3c that annealing the clusters formed from a 4 MLE Pd coverage to 650 K and cooling to room temperature has no appreciable effect on the size distribution or density. Similarly, the Pd/Mo AES intensity ratios measured before and after annealing and cooling are essentially unchanged, consistent with the STM images of Figures 3b and 3c.

Figure 4a shows the PM-IRAS data for CO adsorption on $Pd/SiO_2/Mo(112)$ at 185 mbar between 300 and 600 K. For this spectral series, CO was dosed at 300 K until a pressure of 185 mbar was achieved and then held constant throughout the experiment. The temperature of the surface in the ambient CO environment was then raised successively, and in-situ PM-IRAS data were collected. The topmost spectrum in Figure 4a (PM-IRAS at 300 K) shows two prominent, complex bands centered at approximately 2089 and 1957 cm $^{-1}$ in addition to two other less prominent features at ~2009 and ~1895 cm^{-1}. As the temperature of the catalyst is increased, the IR band at 2089 cm^{-1} with an asymmetry toward the low-frequency side

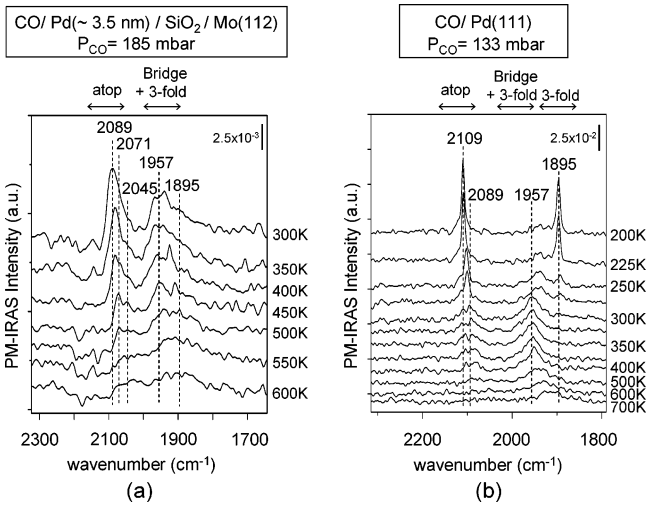

Figure 4. In-situ PM-IRAS data for CO adsorption on silica-supported Pd nanoclusters (a) in comparison with the Pd(111) single-crystal surface (b). All of the spectra are obtained in the presence of the high-pressure CO gas phase at the given temperatures.

exhibits a monotonic decrease in intensity as well as a red shift of its vibrational frequency to 2071 cm^{-1} at 600 K. In addition, an increase in the catalyst temperature accentuates the asymmetry of the IR feature at 2089 cm^{-1}; at 450 K this feature eventually splits into two distinct peaks at 2071 and 2045 cm^{-1}. The other complex band, centered at approximately 1957 cm^{-1}, decreases in intensity and red shifts to ~1900 cm^{-1} following an increase in the surface temperature to 600 K.

Figure 4b shows in-situ PM-IRAS data for CO adsorption on Pd(111) at 133 mbar. The series of spectra in Figure 4b were acquired under similar conditions as were the data of Figure 4a; however, the initial gas dosing was carried out at 600 K, then the surface temperature was lowered successively while keeping the CO pressure in the IR microreactor constant at 133 mbar. At 200 K, sharp features at 2109 and 1895 cm^{-1} dominate the spectrum. As the temperature is increased, the intensity of the feature at 2109 cm^{-1} decreases continuously while red shifting to 2085 cm^{-1} at 350 K; eventually its intensity essentially disappears at 500 K after red shifting to ~2075 cm^{-1}. The second prominent feature at 1895 cm^{-1} is at 200 K in Figure 4b and decreases in intensity with an increase in temperature with essentially no change in the peak position. Beside these two prominent IR bands, a C−O stretching feature appears at ~1930 cm^{-1} as the temperature is raised to 250 K with a

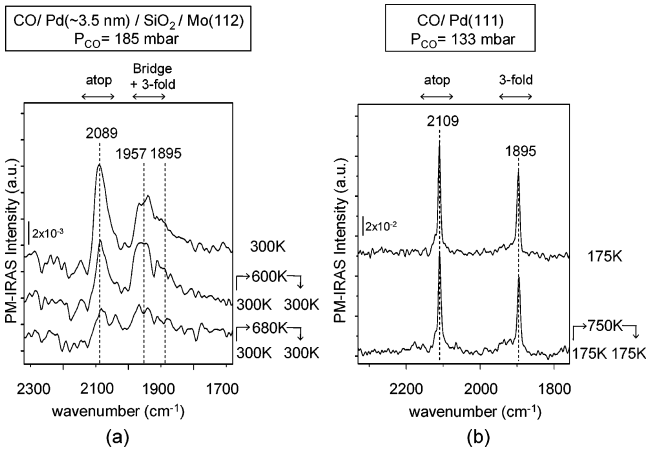

Figure 5. In-situ PM-IRAS data showing the response of the vibrational features for the adsorbed CO on the silica-supported Pd nanoclusters (a) and the Pd(111) single-crystal surface (b) to annealing−cooling cycles. See text for details.

concomitant blue shift to 1957 cm^{-1} at 350 K. Above 350 K, the frequency of this feature shifts to ∼1930 cm^{-1}.

Figure 5 shows a series of spectra highlighting the reversibility/irreversibility of the vibrational features of CO adsorption versus temperature for silica-supported Pd nanoclusters compared with a Pd(111) single crystal. In this set of experiments, CO was dosed, then the surface was heated in the presence of an elevated pressure of CO. The surface was then cooled to the original temperature, and the spectrum was compared with the initial spectrum. The upper spectrum in Figure 5a shows the CO spectral features for silica-supported Pd nanoclusters at 300 K with a CO pressure of 185 mbar. As mentioned above, two major C−O stretching bands at 2089 and 1957 cm^{-1} are present under these conditions. In the first anneal−cool cycle, Pd nanoclusters are annealed to 600 K and cooled rapidly to 300 K. It is clear from the middle spectrum of Figure 5a that this temperature treatment has an irreversible effect on the PM-IRA spectrum, i.e., there is considerable attenuation of the total IR intensity of the 2089 cm^{-1} feature by approximately 35% with essentially no effect on the band at 1957 cm^{-1}. Repeating this temperature program (with an increase in the anneal temperature to 680 K) causes a greater attenuation of the band at 2089 cm^{-1} and attenuates its intensity by 75%. Furthermore, this second temperature treatment leads to a profound decrease in the total IR intensity of the band at 1957 cm^{-1} by approximately 60%. In addition to these observations, the AES spectrum after the temperature program indicates a considerable amount of C deposition on the surface (Figure 6). The inset in Figure 6 is a difference spectrum of the AES for Pd nanoclusters before and after 185 mbar CO exposure at 600 K. The feature at 271 eV in the difference AES corresponds to C. The line shape of this AES feature suggests a carbide-like nature for this C species. In contrast to Pd nanoclusters, a similar temperature treatment has no significant influence on the vibrational spectrum of adsorbed CO on Pd(111) at 133 mbar where almost all (93%) of the vibrational features observed at 175 K are recovered after annealing to 750 K in the presence of 133 mbar of CO gas and cooling to 175 K. Reversibility of the Pd(111) surface with respect to CO adsorption at elevated pressures is also visible in the AES data (Figure 7) obtained for Pd(111) surfaces before and after 133 mbar CO exposure (175−750 K). It should be noted that for both Pd(111) and supported Pd nanoparticle surfaces, evacuation of the reactor was performed under identical conditions at room temperature and AES were acquired after

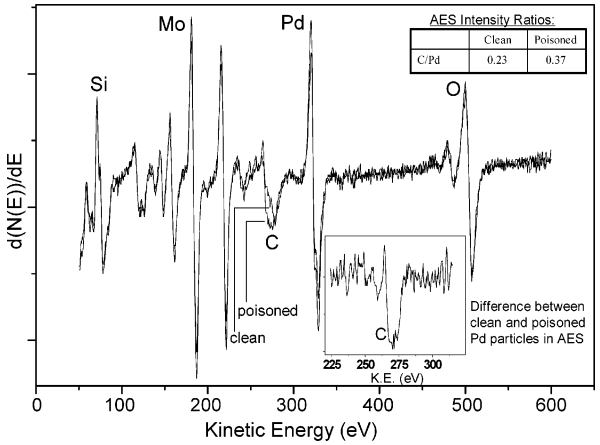

Figure 6. Auger electron spectra for silica-supported Pd nanoparticles before and after 185 mbar CO exposure. Spectrum in the inset shows the difference between the AES for clean and poisoned Pd particles. Spectrum for the clean surface was obtained immediately after Pd deposition on SiO_2 film and the spectra for the exposed Pd particles were obtained after 185 mbar CO exposure, evacuation at 300 K, and successive annealing at 600 K in UHV.

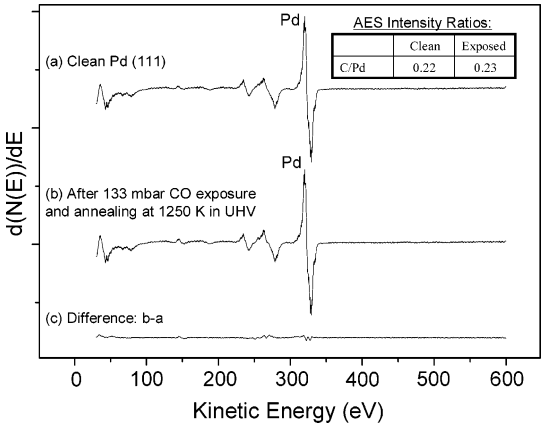

Figure 7. (a) AES for clean Pd(111) surface. (b) AES for Pd(111) surface exposed to 133 mbar CO and subsequently annealed at 1250 K in UHV. (c) Difference between the Auger electron spectra given in (a) and (b).

annealing the Pd surfaces in UHV to desorb molecularly adsorbed CO species.

In a similar control experiment, 133 mbar of CO was dosed on a pristine SiO_2 thin film without Pd deposition. No PM-IRAS features associated with any adsorbed CO species on SiO_2 film were detected. Furthermore, AES data obtained for the SiO_2 film before and after 133 mbar CO exposure showed no indication for C formation on clean SiO_2 film (Figure 8).

IV. Discussion

Previous vibrational spectroscopic studies on CO adsorption on Pd clusters deposited on amorphous SiO_2 indicate that the silica-supported Pd clusters exhibit primarily ⟨111⟩ and ⟨100⟩ facets.[26] Therefore for relatively large metal clusters, CO adsorption on Pd single-crystal surfaces can be utilized to explain some of the aspects of CO adsorption. On a Pd(111) single-crystal surface, CO forms various coverage-dependent ordered overlayers that have been studied extensively.[21,29−31] At a CO coverage of $\theta_{CO} = 0.33$ ML, a CO ordered overlayer with a $(\sqrt{3} \times \sqrt{3})$ R 30° − 1CO structure is the dominant phase where CO resides primarily on 3-fold hollow sites. This yields a distinctly low C−O vibrational frequency of ∼1850 cm^{-1}.[21,29−31]

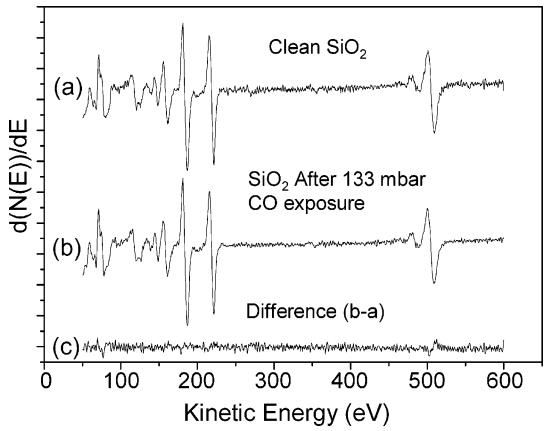

Figure 8. (a) AES for clean SiO_2 ultrathin film grown on Mo(112) substrate. (b) AES for SiO_2/Mo(112) after 133 mbar CO exposure and evacuation at RT. (c) Difference between the Auger electron spectra given in (a) and (b).

As the CO coverage is increased to $\theta_{CO} = 0.50$ ML, the CO overlayer structure is dominated by two coexisting c(4 × 2)-2CO phases where CO resides either in the bridging sites or in the 3-fold hollow sites.[30] This structure yields a C−O vibrational frequency of ∼1920 cm^{-1}.[21,29−31] Between $\theta_{CO} = 0.50$ and 0.75 ML, complex overlayer structures are observed which result in a CO vibrational band near 1965 cm^{-1}. Recent STM experiments combined with DFT calculations suggest that CO occupies primarily bridging sites on the Pd(111) surface within this coverage regime.[30] Finally at $\theta_{CO} = 0.75$ ML, saturation CO coverage is obtained with a (2 × 2)-3CO structure where CO is found on both atop and 3-fold hollow sites corresponding to vibrational features at 2110 and 1895 cm^{-1}, respectively.[21,29−31] In a recent PM-IRAS study,[9] it was demonstrated that CO overlayers follow similar trends in the observed vibrational frequencies within the pressure regime 10^{-6}−600 mbar, implying that no new pressure-induced species or adsorbate-induced surface reconstructions occur on the Pd(111) surface during CO adsorption at elevated pressures.

On the Pd(100) surface, only bridged-site adsorption is observed throughout the coverage range ($\theta_{CO} = 0$−0.81 ML) where the CO vibrational band shifts continuously from 1895 to 1997 cm^{-1}, yielding an ordered overlayer structure of ($2\sqrt{2} \times \sqrt{2}$) R45° − 2CO at $\theta_{CO} = 0.5$ ML.[29] At coverages higher than 0.5 ML, various incommensurate overlayers are observed due to uniaxial compression.[32,33]

The PM-IRAS data shown in Figures 4 and 5 can be explained in light of the above. A detailed discussion of the PM-IRAS data presented in Figure 4b was reported in a previous study.[9] Some important aspects of the spectra are as follows. Introducing 133 mbar of CO to a Pd(111) single-crystal surface and lowering the temperature to 200 K leads to a saturation coverage of $\theta_{CO} = 0.75$ ML and a (2 × 2)-3CO overlayer structure. This (2 × 2)-3CO structure yields vibrational features at 2109 and 1895 cm^{-1} that correspond to adsorption on atop and 3-fold-hollow sites, respectively. Within the temperature range 300−500 K, bridging adsorption features in the PM-IRA spectra are found to be prominent with a C−O stretching frequency at approximately 1957 cm^{-1} which shifts to lower values with increasing temperature (or decreasing CO coverage). Also in this temperature range, there is a minor contribution from atop CO species, although this feature is relatively low in intensity and at a lower vibrational frequency (∼2089 cm^{-1}). With a decrease in the CO coverage on Pd(111) by an anneal to >600 K, CO molecules move to 3-fold hollow sites to form a mixed c(4 × 2)-2CO phase consisting of CO molecules adsorbed on both bridging and 3-fold hollow sites. The coverage at this point is approximately 0.5 ML, and the CO exhibits a stretching frequency of ∼1920 cm^{-1}.

A comparison of Figure 4a of the PM-IRA spectra for CO adsorption on silica-supported Pd nanoclusters with Figure 4b, corresponding to CO adsorption on Pd(111) between 300 and 600 K, shows an interesting similarity, consistent with the silica-supported Pd nanoclusters consisting primarily of ⟨111⟩ facets. In Figure 4a, exposure of the Pd clusters to 185 mbar of CO at 300 K leads to two complex bands at 2089 and 1957 cm^{-1}. On the basis of the above discussion, the band centered at 2089 cm^{-1} can be assigned to a C−O stretching mode of a CO species adsorbed on the atop sites of the ⟨111⟩ facets of the Pd nanoclusters. Furthermore, the asymmetry in the low-frequency edge of this band shows structures at approximately 2071 and 2045 cm^{-1}. These additional features are probably related to the three-dimensional structure of the Pd nanoclusters with heterogeneous sites for CO adsorption, e.g., steps or other defect sites. In a recent IRAS study of CO adsorption on Pd/SiO_2/Mo(112), a feature at 2078 cm^{-1} was also observed and assigned to the CO molecules adsorbed on top of Pd atoms at the step-edge.[21] The relatively lower frequency of this species was suggested to be a consequence of the increased π-back-donation from the coordinatively unsaturated Pd atoms at the steps. The feature at 2071 cm^{-1}, Figure 4a, then, is assigned to CO residing on step-edge-like atoms of the Pd clusters.

It is shown in Figure 4a that at 450 K, the intensity of the feature at 2089 cm^{-1} due to an atop CO species on ⟨111⟩ facets virtually disappears, whereas the band at 2071 cm^{-1} is still visible, suggesting that CO binds to atop sites of the ⟨111⟩ facets of the Pd clusters less strongly than to step-edge atoms. At higher temperatures, CO adsorption onto atop sites of the ⟨111⟩ facets is less favored.

The feature at 2045 cm^{-1} can be assigned to CO molecules occupying bridging sites of the Pd clusters that are possibly on or near extended defects such as steps. This point will be addressed in more detail during the discussion of Figure 5a and Figure 5b below.

In addition, the vibrational feature observed at 1957 cm^{-1} in Figure 4a can be readily assigned to CO molecules occupying bridging sites of the ⟨111⟩ facets by comparing the uppermost spectrum in Figure 4a with the spectrum acquired at 300 K in Figure 4b. The shoulder observed at 1895 cm^{-1} in Figure 4a can be assigned to CO adsorption on the 3-fold hollow sites of the ⟨111⟩ facets. In addition to this feature, a minor vibrational feature at ∼2009 cm^{-1} is assigned to CO residing on the bridging sites of ⟨100⟩ facets. The ⟨100⟩ facets have been shown to contribute only to a small extent to the overall structure of small silica-supported Pd nanoclusters. While Pd clusters on crystalline SiO_2 with an average of 850 atoms/cluster show a relatively large contribution from ⟨100⟩ facets in the vibrational spectrum of adsorbed CO, Pd clusters with 110 atoms/cluster show almost no contribution from ⟨100⟩ facets.[21] On the basis of the STM image shown in Figure 3b, the average Pd cluster diameter and height are 3.5 and 0.7 nm, respectively. From these dimensions, the average number of Pd atoms/cluster can be estimated to be approximately 330.

Although the spectrum obtained at 300 K in Figure 4a displays important similarities with respect to the spectrum obtained at 300 K in Figure 4b, there are significant differences that are noteworthy. It is apparent from Figure 4a that at 300 K the CO adsorption on atop sites of Pd nanoclusters occurs to a greater extent than adsorption on multiply coordinated sites in

contrast to adsorption on Pd(111). This can be rationalized by considering the three-dimensional geometry of the Pd clusters. From the STM images in Figure 3 it can be easily seen that in contrast to an atomically flat Pd(111) single-crystal surface, Pd nanoclusters deposited on crystalline SiO_2 have curvature with various surface defects and lack flat and ordered terraces for CO adsorption.

Further important insights can arise by studying the interaction between adsorbed CO and Pd at elevated temperatures and pressures. Figure 5b and Figure 7 imply that an ordered (2×2)-3CO overlayer, once formed on Pd(111), is not affected by an anneal−cool cycle in the presence of high-pressure CO gas, i.e., no observed new state or species, adsorbate-induced surface reconstruction, or CO dissociation. It should be noted that as the (2×2)-3CO state forms at a saturation coverage of $\theta_{CO} = 0.75$ ML on Pd(111), any significant amount of CO dissociation accompanied by the blocking of the Pd(111) adsorption sites should be readily visible via a pronounced distortion or probably disappearance of this ordered adsorbate overlayer to form a more disordered state; however, Figure 5b clearly indicates that this is not the case. That no CO dissociation on Pd(111) occurs is supported by recent DFT calculations where the activation energy for CO dissociation on Pd(111) is reported to be much higher than that for Pd defect sites such as steps or kinks.[34,35] Although the absolute values of the activation energies reported in these separate DFT studies differ, both studies consistently show a significantly higher activation energy for CO dissociation on Pd(111) terrace sites (4.4 eV[34] or 1.87 eV[35]) compared with defects sites such as steps (3.5 eV[34] or 0.57 eV[35]) and kinks (0.38 eV)[35]. Although these conclusions regarding CO adsorption on Pd(111) at elevated pressures exclude CO dissociation, recent elevated-pressure SFG experiments performed by Somorjai and co-workers on Pt(111) report C deposition on the Pt(111) surface due to CO dissociation during CO adsorption on Pt(111)[36] and $CO + O_2$ reaction at 673 K.[37]

Figure 5a clearly points out that the silica-supported Pd nanoclusters undergo an irreversible change when the surface is annealed to a high temperature in the presence of 185 mbar of CO. There are several explanations for these findings; however, one that can be excluded is a change in the morphology of the Pd nanoclusters due to the annealing procedure since no morphological change is seen in the STM images of Figure 3b and Figure 3c. In addition, AES data given in Figure 6 reveal that for the silica-supported Pd nanoparticles the Pd/Mo intensity ratio stays relatively intact even after 185 mbar CO exposure within 300−680 K (Pd/Mo was 0.85 and 0.79 for clean and exposed surfaces, respectively). On the basis of our previous studies, morphological changes of the Pd nanoclusters via sintering and/or inter-diffusion occur above 700 K.[20] Therefore, one of the plausible explanations is the dissociation of CO on the Pd nanoclusters and subsequent poisoning of the CO adsorption sites on the Pd nanoclusters by the dissociation products (i.e., atomic C and O). CO dissociation by silica-supported Pd clusters on a high surface area Pd/SiO_2 catalyst has been reported by Boudart and co-workers[38] as well as others for various Pd surfaces.[39−41] As discussed above, because of their three-dimensional geometry, Pd nanoclusters exhibit a high density of surface defects such as steps or kinks that can bind CO molecules more strongly than nondefect sites on ⟨111⟩ or ⟨100⟩ terraces and hence activate C−O bond scission. The activity of the defect sites on Pd surfaces toward dissociation of CO are supported by recent DFT calculations that are mentioned above.[34,35] Furthermore, our AES results that show formation of a C deposit after an anneal-cool cycle are consistent with CO dissociation. It should also be emphasized that the evidence for CO dissociation discussed in this report is found at elevated pressures. Under lower pressure conditions such as 10^{-5} mbar, our PM-IRAS results, which are not shown here, suggest that CO adsorbs mostly in a molecular fashion on the supported Pd particles, consistent with the previous adsorption experiments in the literature under similar conditions.[21] Although there is a possibility of impurity species in the gas background giving rise to the observed results, no vibrational or electron spectroscopic evidence for the presence of a minority species (any species other than CO) was detected on the Pd surfaces in our experiments

Another interesting aspect of Figure 5a is the behavior of the vibrational bands centered at 2089 cm^{-1} (corresponding to atop and bridging sites) and at 1957 cm^{-1} (corresponding to bridging and 3-fold hollow sites) to successive temperature treatments. Although there is a total intensity attenuation of 35% for the atop/bridging CO species (2089 cm^{-1}) after the first annealing−cooling cycle, the total IR signal for the bridging/3-fold hollow sites (1957 cm^{-1}) remains unchanged. This suggests that CO molecules residing on the bridging or atop sites of the steps of the Pd nanoclusters are likely to be responsible for CO dissociation. After CO dissociation on these defect sites, atomic C and O diffuse to the neighboring atop (2089 and 2071 cm^{-1}) and bridging sites (2045 cm^{-1}) in *close proximity* to the active sites. Attenuation of the broad vibrational band at 2089 cm^{-1} then occurs. In a second anneal−cool cycle, further CO dissociation leads to spill-over of atomic C and O over the entire Pd cluster, resulting in nonselective attenuation of all vibrational features and to complete poisoning of the Pd clusters.

To support the above arguments, control experiments were carried out by adsorbing CO on a freshly grown crystalline SiO_2 film on Mo(112). CO pressures to 133 mbar at 300 K over a SiO_2/Mo(112) surface produced no PM-IRAS signal corresponding to C−O or any C deposition on the SiO_2 film was observed before or after CO exposure (Figure 8). Also, AES data presented in Figures 6 and 8 exclude the occurrence of some other surface phenomena such as adsorbate-induced segregation of the substrate Mo atoms to the surface causing subsequent CO dissociation. These results indicate that CO adsorption does not take place on the SiO_2 film under these conditions, nor is there any adsorption on the underlying Mo(112).

V. Conclusions

Our combined STM and in-situ PM-IRAS results reported in this study can be summarized as follows:

(a) CO adsorbs molecularly and reversibly on Pd(111) even at elevated temperatures (300−750 K) and pressures (133 mbar) with no evidence of CO dissociation.

(b) Combined STM and PM-IRAS data for Pd nanoclusters with an average diameter and height of 3.5 nm and of 0.7 nm, respectively, show mainly ⟨111⟩ facets with a small contribution from ⟨100⟩ facets. Furthermore, temperature-dependent STM results presented in this work show no evidence for a significant change in the cluster morphology or number density between 300 and 650 K for a Pd coverage of 4 MLE.

(c) In-situ PM-IRAS data for CO adsorption on silica-supported Pd nanoclusters indicate that CO at 185 mbar dissociates above 600 K. A comparison with the PM-IRAS data for CO adsorption on an atomically flat Pd(111) single-crystal surface under similar conditions shows that the active sites for

the CO dissociation are defect sites on the Pd clusters, e.g., steps or kinks, due to the high curvature of Pd nanoclusters.

Acknowledgment. This work was supported by the Department of Energy, Office of Basic Energy Sciences, Division of Chemical Sciences, the Robert A. Welch Foundation, and the Texas Advanced Technology Program under Grant No. 010366-0022-2001. The authors acknowledge Dr. J. Wang for helpful discussions.

References and Notes

(1) Nieuwenhuys, B. E. *Adv. Catal*. **2000**, *44*, 259.
(2) Goodman, D. W. *J. Phys. Chem*. **1996**, *100*, 13090.
(3) Goodman, D. W. *Chem. Rev*. **1995**, *95*, 523.
(4) Rider, K. B.; Hwang, K. S.; Salmeron, M.; Somorjai, G. A. *J. Am. Chem. Soc*. **2002**, *124*, 5588.
(5) Hendriksen, B. L. M.; Frenken, J. W. M. *Phys. Rev. Lett*. **2002**, *89*, 046101.
(6) Hansen, K. H.; Sljivancanin, Z.; Hammer, B.; Laegsgaard, E.; Besenbacher, F.; Stensgaard, I. *Surf. Sci.* **2002**, *496*, 1.
(7) Somorjai, G. A.; McCrea, K. R. *Adv. Catal.* **2000**, *45*, 385, and references therein.
(8) Chinta, S.; Choudhary, T. V.; Daemen, L. L.; Eckert, J.; Goodman, D. W. *Angew. Chem., Int. Ed*. **2002**, *41*, 144, and references therein.
(9) Ozensoy, E.; Meier, D. C.; Goodman, D. W. *J. Phys. Chem. B* **2002**, *106*, 9367, and references therein.
(10) Ozensoy, E.; Hess, C.; Goodman, D. W. *J. Am. Chem. Soc*. **2002**, *124*, 8524.
(11) Hess, C.; Ozensoy, E.; Goodman, D. W. *J. Phys. Chem. B* **2003**, *107*, 2759.
(12) Green, M. J.; Barner, B. J.; Corn, R. M. *Rev. Sci. Instrum*. **1991**, *62*, 1426.
(13) Kunimatsu, K.; Golden, W. G.; Seki, H.; Philpott, M. R. *Langmuir* **1985**, *1*, 245.
(14) Blaudez, D.; Turlet, J. M.; Dufourcq, J.; Bard, D.; Buffeteau, T.; Desbat, B. *J. Chem. Soc., Faraday Trans*. **1996**, *92*, 525.
(15) Barner, B. J.; Green, M. J.; Saez, E. I.; Corn, R. M. *Anal. Chem.* **1991**, *63*, 55.
(16) Henrich, V. E.; Cox, P. A. *The Surface Science of Metal Oxides*; Cambridge University Press: Cambridge, 1994.
(17) Heck, R. M.; Farrauto, R. J. *Catalytic Air Pollution Control: Commercial Technology*; International Thomson Publishing: New York, 1995.
(18) Schroeder, T.; Giorgi, J. B.; Baumer, M.; Freund, H. J. *Phys. Rev. B* **2002**, *66*, 165422.
(19) Schroeder, T.; Adelt, M.; Richter, B.; Naschitzki, M.; Baumer, M.; Freund, H. J. *Surf. Rev. Lett.* **2000**, *7*, 7.
(20) Min, B. K.; Santra, A. K.; Goodman, D. W. *Catal. Today* **2003**, *85*, 113.
(21) Giorgi, J. B.; Schroeder, T.; Baumer, M.; Freund, H. J. *Surf. Sci.* **2002**, *498*, L71.
(22) Kim, Y. D.; Wei, T.; Goodman, D. W. *Langmuir* **2003**, *19*, 354.
(23) Kim, Y. D.; Wei, T.; Stultz, J.; Goodman, D. W. *Langmuir* **2003**, *19*, 1140.
(24) Kim, Y. D.; Stultz, J.; Wei, T.; Goodman, D. W. *J. Phys. Chem. B* **2003**, *107*, 592.
(25) Luo, K.; Kim, D. Y.; Goodman, D. W. *J. Mol. Catal. A: Chemical* **2001**, *167*, 191.
(26) Xu, X. P.; Szanyi, J.; Xu, Q.; Goodman, D. W. *Catal. Today* **1994**, *21*, 57.
(27) Xu, X.; He, J.-W.; Goodman, D. W. *Surf. Sci.* **1993**, *284*, 103.
(28) Schroeder, T.; Giorgi, J. B.; Hammoudeh, A.; Magg, N.; Baumer, M.; Freund, H. J. *Phys. Rev. B* **2002**, *65*, 115411.
(29) Hoffmann, F. M. *Surf. Sci. Rep*. **1983**, *3*, 107, and references therein.
(30) Rose, M. K.; Mitsui, T.; Dunphy, J.; Borg, A.; Ogletree, D. F.; Salmeron, M.; Sautet, P. *Surf. Sci.* **2002**, *512*, 48.
(31) Kuhn, W. K.; Szanyi, J.; Goodman, D. W. *Surf. Sci.* **1992**, *274*, L611.
(32) Szanyi, J.; Kuhn, W. K.; Goodman, D. W. *J. Vac. Sci. Technol. A* **1993**, *11*, 1969.
(33) Behm, R. J.; Christmann, K.; Ertl, G.; Van Hove, M. A. *J. Chem. Phys.* **1980**, *73*, 2984.
(34) Hammer, B. *J. Catal*. **2001**, *199*, 171.
(35) Li, Z. P.; Hu, P. *J. Am. Chem. Soc*. **2003**, *125*, 1958.
(36) McCrea, K. R.; Parker, J. S.; Somorjai, G. A. *J. Phys. Chem. B* **2002**, *106*, 10854.
(37) Kung, K. Y.; Chen, P.; Wei, F.; Shen, Y. R.; Somorjai, G. A. *Surf. Sci*. **2000**, *463*, L627.
(38) Ichikawa, S.; Poppa, H.; Boudart, M. *J. Catal.* **1985**, *91*, 1.
(39) Rainer, D. R.; Wu, M. C.; Mahon, D. I.; Goodman, D. W. *J. Vac. Sci. Technol. A* **1996**, *14*, 1184.
(40) Matolin, V.; Gillet, E. *Surf. Sci.* **1990**, *238*, 75.
(41) Johanek, V.; Stara, I.; Matolin, V. *Surf. Sci*. **2002**, *507*, 92.